JPSE (Journal of Physical Science and Engineering), Vol. 7, No. 2, 2022, Page 86–91.
DOI: 10.17977/um024v7i22022p086

JPSE
(Journal of Physical Science and Engineering)

http://journal2.um.ac.id/index.php/jpse
EISSN: 2541-2485

Investigation of Optical Properties and Electronic Transfer of Temperature-Dependent ZnO Nanocolumnars Grown by DC Sputtering

Received
16 September 2022

Revised
10 Ocotober 2022

Accepted for Publication
12 October 2022

Published
24 October 2022

R Kurniawan[1*], I S M Sari, I Yulianingtyas[1], J P Setyawan[1], I N A Dahlan[1], R Marlina[2], and J Suwardy[3]

1. Department of Physics, Faculty of Mathematics and Natural Sciences, Universitas Negeri Malang, Jl. Semarang No. 5, Malang, 65145, Indonesia.
2. Research Center for Biomass and Bioproducts, National Research and Innovation Agency, Jl. Raya Bogor km 46, Bogor, 16911, Indonesia.
3. Research Center for Quantum Physics, National Research and Innovation Agency, Jl. Kawasan Puspiptek, South Tangerang, 15314, Indonesia.

***E-mail:** robi.kurniawan.fmipa@um.ac.id

Abstract
The morphology of zinc oxide (ZnO) can determine the distribution of defects in the system, which plays an important role in determining its optical and electronic properties. Here, we investigate the optical and electronic transfer properties of different ZnO surface morphologies. ZnO nanocolumnar was synthesized by direct-current (DC) sputtering followed by annealing using a ratio of T/Tm = 0.15, 0.20, and 0.25. The x-ray diffraction (XRD) results show that an increase in annealing temperature causes an increase in crystal size accompanied by a decrease in lattice strain. Furthermore, the surface morphology of the sample changed with increasing annealing temperature treatment, following the structural zone model. The optical and electronic transfer properties of the samples were investigated in three regions; region 1 (T/Tm = 0.15), region 2 (T/Tm = 0.20), and region 3 (T/Tm = 0.25) using optical modeling. The highest surface electronic transfer was noted in region 2, which is indicated by the highest surface energy loss function (SELF). This research can provide a good understanding in designing optoelectronic systems based on their morphological features.
Keywords: ZnO nanocolumnar, DC sputtering, structural zone model, SELF.

1. Introduction

In optoelectronic applications, the performance of a system depends on a superior level of stability, sensitivity, and responsivity. For example, the materials used in the design of solar cells and photodetectors are semiconductor materials that have absorption capabilities in the visible and UV ranges, such as zinc oxide (ZnO) [1], [2] and titanium dioxide (TiO_2) [3], [4]. Here, light absorption and electron transfer in semiconductor materials can be controlled, either by modifying their structure and morphology [5], [6].

ZnO is a potential material for optoelectronic application because it has excellent optical and electronic properties, with electron mobility of 205–300 for bulk and 1000 $cm^2V^{-1}s^{-1}$ for ZnO nanorods [2]. ZnO is an n-type semiconductor that is widely used in optoelectronic applications because it has good stability at room temperature. ZnO has been used for several parts of solar cells, such as for the active layer, which functions to absorb sunlight [7], and the electron transfer layer (ETL) [8], which functions to transfer electrons from the active layer to the electrodes [9], [10]. In solar cell applications, ZnO has a fast recombination rate, which is undesirable [11], [12]. To improve the performance of ZnO in solar cell applications, it is necessary to avoid electron recombination, which can be accomplished by the use of doping systems, modification of defects, formation of composite systems, and the addition of other layers. The presence of defects in the system plays a role in presenting the characteristics of light absorption in a certain wavelength range. Defects in the system can be modified through morphological settings. In one-dimension (1D) materials, the reduction in diameter will increase the surface-to-volume ratio (SVR) of the system [13]. This increase in SVR is associated with an increase in the total surface area of the system, which will result in a distributed defect on the surface [14].

In this study, the surface morphology of ZnO will be investigated at different annealing temperatures. Furthermore, the optical properties of ZnO will be comprehensively analyzed using optical modeling. These results will provide a good understanding of the technique of modifying morphology and changes in its characteristics. Determination of morphology and suitable optical properties can be used in designing optoelectronic-based devices that can be tailored to the needs, with good performance.

2. Method

ZnO samples were deposited on silicon (Si) substrates using direct-current (DC) sputtering. The Zn target was bombarded by argon (Ar) under an oxygen (O_2) atmosphere, with an Ar-O_2 flow of 45-10 sccm. The deposition was performed for 15 minutes at room temperature by using chamber pressure and the deposition power of 1×10^{-2} Pa and 80 W, respectively. The samples were then annealed at various temperatures to obtain values of T/Tm = 0.15, 0.20, and 0.25, where T was the annealing temperature and Tm was the melting point of ZnO (1975 °C) [15], [16]. The crystal structure was characterized by x-ray diffraction (XRD) PANalytical X'Pert Pro. Morphological modifications, including distribution, were studied through the surface and cross-sectional images using scanning electron microscopy (SEM) FEI: INSPECT S50. Subsequently, fluorescence measurements and spectroscopic ellipsometry characterization Micropack: Spec-El 2000 were used to investigate the optical and electronic transfer properties of the samples.

3. Result and Discussion

Figure 1 shows the diffraction pattern of the sample with different variations of annealing temperature. We confirmed that ZnO has a hexagonal wurtzite structure with the intensity of the diffraction peaks changing with variations in the annealing temperature. Increasing the annealing temperature will provide energy into the system that plays a role in crystal construction. The detail of crystal properties, including crystal size (D) and lattice strain (ε), is presented in Table 1.

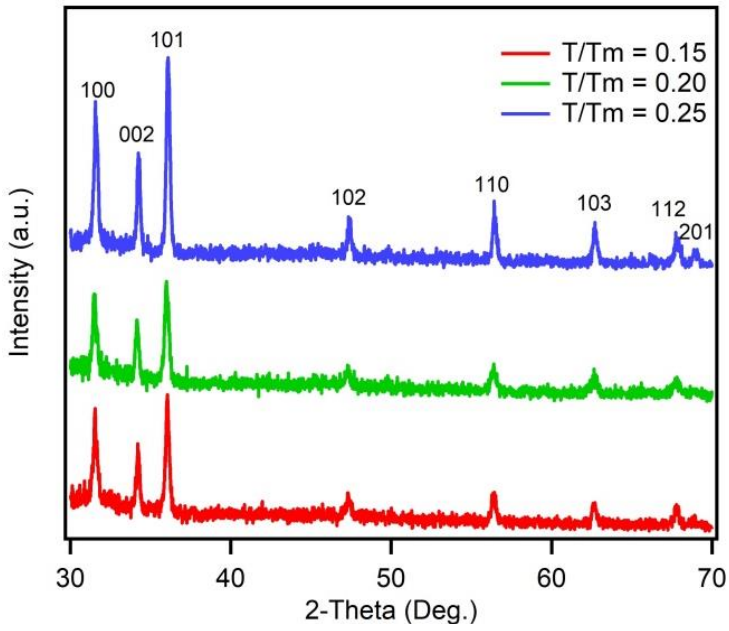

Figure 1. Diffraction pattern of ZnO nanocolumnars with different annealing temperatures.

Table 1. Crystal size and lattice strain of the samples.

Sample name	Full width at half maximum/FWHM (°)	Crystal size (nm)	Lattice strain (10^{-3})
T/Tm = 0.15	0.39934	20.68	6.17
T/Tm = 0.20	0.38862	21.25	6.01
T/Tm = 0.25	0.31692	26.06	4.89

The results showed that an increase in annealing temperature caused an increase in crystal size accompanied by a decrease in lattice strain. This condition can be explained by the structural zone model approach, where the sample with T/Tm = 0.15 to 0.25 are dominated by diffusion and crystal growth processes. This condition is characterized by an increase in crystal size and a more stable crystal state (decreased lattice strain). We noted a decrease in the diffraction peak for T/Tm = 0.20, which is presumably due to fluctuations in the system state and the presence of a defect [17].

Figure 2a shows the surface morphology of the top view and side view samples measured by SEM. The surface mapping results confirmed that the sample had uniform growth, which was indicated by the yellow population area. This uniform growth indicates that the sample has a low level of roughness. Surface morphology investigations were also carried out in the regions along the crystal growth. Here, we note that the sample has a non-uniform shape, where the upper side is larger than the lower side, forming a cone-like shape. Figure 2b shows an illustration of the structural zone model of the sample. Here, it can be divided into three regions; region 1 (T/Tm = 0.15), region 2 (T/Tm = 0.20), and region 3 (T/Tm = 0.25). Region 1 to the edge of region 2 (T/Tm < 0.20) is the first nucleation area for the material to grow upwards to form vertically arranged columns with homogeneous bottom and top shapes. Regions 2 and 3 are included in the transition region (T-Zone) which is characterized by morphological inhomogeneity along the thickness, forming a V-shape [15], [16]. This is due to the competitive texture due to surface diffusion and grain boundary migration. The presence of defects is estimated to be very large in all these 1–3 regions because the system is still fluctuating towards a more stable system.

To demonstrate the presence of the defect and its influence on the system properties, an analysis of the optical properties has been presented. The electron transfer of the system can be represented by the conductivity spectra, as shown in Figure 3a. A wide range of conductivity spectra in the energy range of 2.7–3.1 eV (visible-UV) was observed. The visible optical conductivity indicated the presence of interband transitions in ZnO, which can originate from the defect states. The presence of defects in the ZnO system has been investigated in a previous report [18], wherein the presence of defects provides an additional state to the system. In addition, the existence of oxygen vacancy (V_O) acts as a double donor, which provides an additional electron to the system and further contributes to the improvement of optical conductivity.

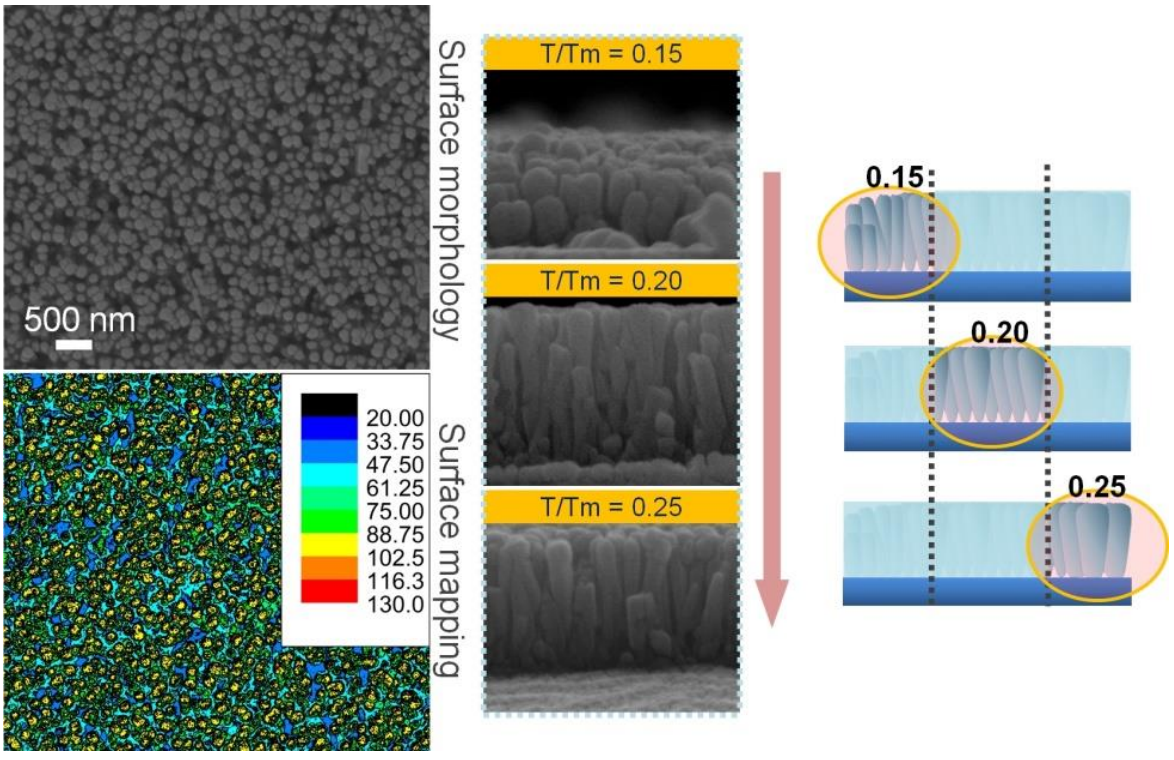

Figure 2. (a) SEM image and (b) schematic illustration of ZnO nanocolumnars with different annealing temperatures.

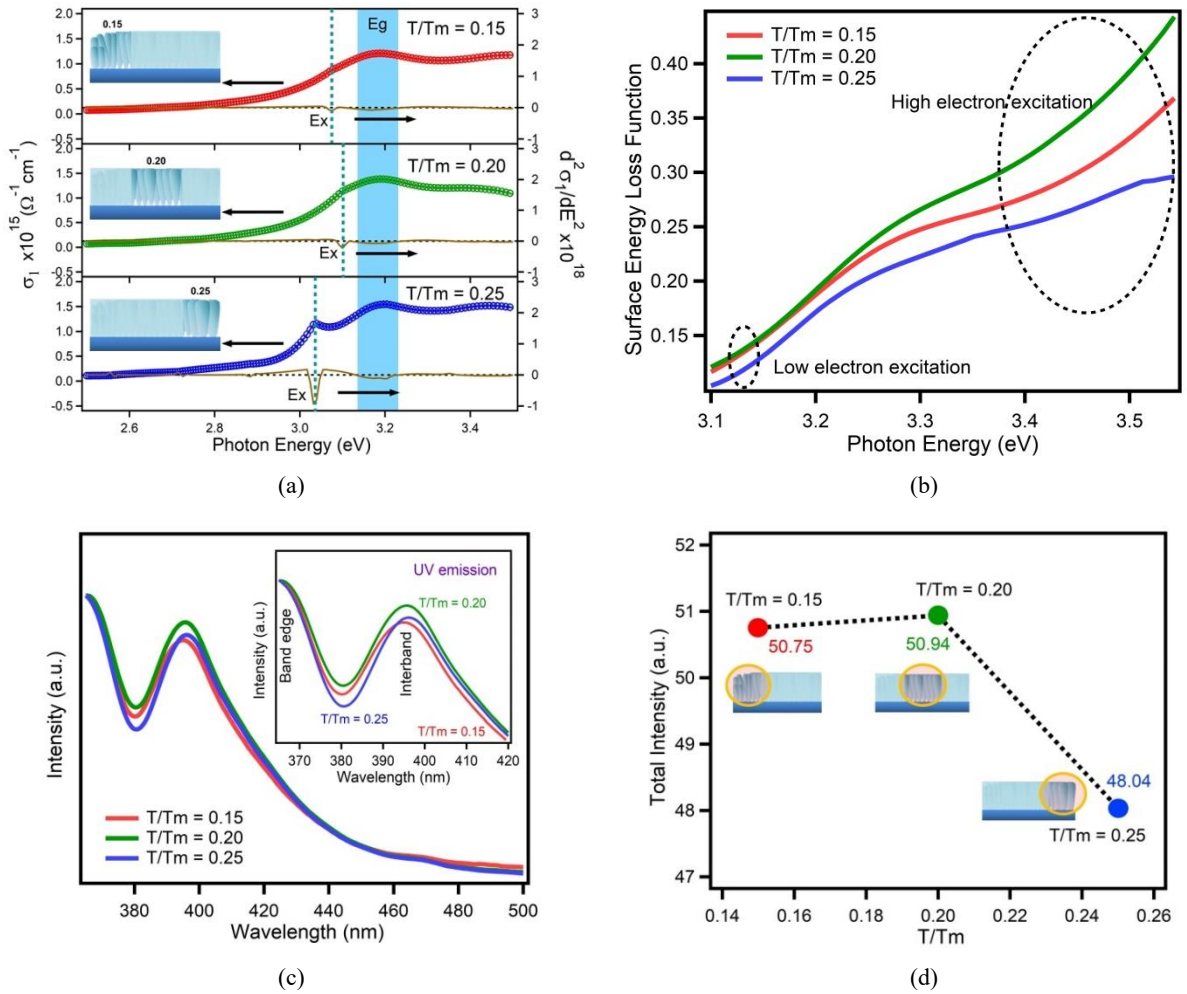

Figure 3. (a) Optical conductivity, (b) surface energy loss function/SELF, and (c), and fluorescence spectra of ZnO nanocolumnars with different annealing temperatures. Inset in Figure (c) presents UV emission region and (d) total (integration) emission.

Generally, ZnO has a native defect of V_O and a small number of other defects such as zinc vacancy (V_{Zn}), zinc interstitial (I_{Zn}), and oxygen interstitial (I_O) [19], [20]. Furthermore, to investigate electron transfer, the second derivative of optical conductivity was presented. A critical point (CP) was observed in all three samples, with a CP of 3.04, 3.10, and 3.08 eV for T/Tm = 0.15, 0.20, and 0.25, respectively. CP indicates the point at which there is a significant improvement in the system. Here, the difference in CP values is thought to be due to the effect of the distribution of defects on the system.

All samples show high electron transfer above the band gap. To investigate electron transfer, a comprehensive analysis is presented. Figure 3b shows the surface energy loss function (SELF) spectra. SELF is determined by the Equation 1 [21], [22],

$$\mathrm{SELF} = \mathrm{Im}\left[\frac{-1}{\varepsilon(\omega)+1}\right] = \frac{\varepsilon_2(\omega)}{\left[1+\varepsilon_1(\omega)\right]^2 + \varepsilon_2{}^2(\omega)} \tag{1}$$

with $\varepsilon(\omega)$ is the complex dielectric function, $\varepsilon_1(\omega)$ the real part of the dielectric function, and $\varepsilon_2(\omega)$ the imaginary part of the dielectric function. SELF characterizes the probability of electrons undergoing surface excitation in the surface region. The sample T/Tm = 0.20 shows the greatest surface excitation than that of the other samples. This result can be explained by the presence of a defect in the system. The presence of defects in the system will play a role in the electron trapping process in the excitation and recombination processes. The high SELF results can be attributed to the distribution of defects in the surface area in the sample T/Tm = 0.20 higher than the other samples. It can also be shown that the

excitation of electrons to the surface region increases with increasing energy. This result is also supported by the previous explanation, where $T/Tm = 0.20$ is a transition area with a high probability of the presence of defects. The sample $T/Tm = 0.25$ shows the lowest SELF due to the restructuring texture, whereas in this zone the sample has homogeneity throughout its thickness and an increase in crystal quality.

Figure 3c shows the fluorescence spectra, which show the emission levels in the sample. The peak pattern with a broadened shape indicates that the emission occurs over a wide range of wavelengths, where both UV and visible light emissions have been observed. Significant differences were observed in the UV region. The inset in Figure 3c shows the emission in the UV range for all samples. Peaks at wavelengths of ~360 and ~390 nm indicate band edge and interband emissions, respectively. A non-monotone trend was observed in the UV emission region, where the fluorescence spectra were independent of increasing temperature. Furthermore, to show the total emission in each sample, intensity integration results have been presented. We note that the total emission values are 50.75, 50.94, and 48.04 for $T/Tm = 0.15$, 0.20, and 0.25, respectively, as shown in Figure 3d. This pattern is in good agreement with the SELF data, where the sample $T/Tm = 0.20$ has the highest total emission.

4. Conclusion

ZnO nanocolumnar has been successfully synthesized on Si substrate using DC sputtering. The increase in annealing temperature caused an increase in crystal size from 20.68 to 26.06 nm accompanied by a decrease in lattice strain from 6.17×10^{-3} to 4.89×10^{-3}. The optical and electronic transfer properties of the three ZnO morphological zones have been investigated using optical modeling. We found that the highest electron transfer was shown by the sample $T/Tm = 0.20$, which was presumably due to the presence of a defect in the system. The SELF spectra confirmed that the sample $T/Tm = 0.20$ had electron excitation in the highest surface region. This is presumably due to the presence of a high defect in the surface area. The presence of this high surface defect can be attributed to the morphology of the samples with $T/Tm = 0.20$ (T-Zone).

Acknowledgment

This research is supported by UM Internal Funding research program and partly funded by RKI 2022 research program.

References

[1] M. Ahmadi, M. Abrari, and M. Ghanaatshoar, "An all-sputtered photovoltaic ultraviolet photodetector based on co-doped $CuCrO_2$ and Al-doped ZnO heterojunction," *Sci. Rep.*, vol. 11, no. 1, p. 18694, Dec. 2021, doi: 10.1038/s41598-021-98273-5.

[2] A. Wibowo *et al.*, "ZnO nanostructured materials for emerging solar cell applications," *RSC Adv.*, vol. 10, no. 70, pp. 42838–42859, Nov. 2020, doi: 10.1039/D0RA07689A.

[3] S. Agrohiya *et al.*, "Fabrication of n-TiO_2/p-Si photo-diodes for self-powered fast ultraviolet photodetectors," *Silicon*, May 2022, doi: 10.1007/s12633-022-01913-2.

[4] Z. Li, Z. Li, C. Zuo, and X. Fang, "Application of nanostructured TiO_2 in UV photodetectors: A review," *Adv. Mater.*, vol. 34, no. 28, p. 2109083, Jul. 2022, doi: 10.1002/adma.202109083.

[5] N. Mufti *et al.*, "Morphological modification and analysis of ZnO nanorods and their optical properties and polarization," *Scanning*, vol. 2018, pp. 1–8, Nov. 2018, doi: 10.1155/2018/6545803.

[6] Y. N. Hendri, R. Kurniawan, K. Takase, and Y. Darma, "Origin of ferroelectricity in carbon-doped ZnO nanocolumnars: Experimental and density-functional studies," *Ceram. Int.*, vol. 48, no. 2, pp. 2038–2044, Jan. 2022, doi: 10.1016/j.ceramint.2021.09.289.

[7] B. Z. Farzin, M. Parhizkar, H. Bidadi, and F. Abbasi, "ZnO nanoparticles and polyaniline blend as an active layer for bulk heterojunction solar cell applications," *J. Mater. Sci.: Mater. Electron.*, vol. 29, no. 21, pp. 18128–18135, Nov. 2018, doi: 10.1007/s10854-018-9924-0.

[8] C. Liu, C. Xiao, and W. Li, "Zinc oxide nanoparticles as electron transporting interlayer in organic solar cells," *J. Mater. Chem. C*, vol. 9, no. 40, pp. 14093–14114, Sep. 2021, doi: 10.1039/D1TC03434K.

[9] I. Ullah *et al.*, "Enhanced efficiency of organic solar cells by using ZnO as an electron-transport layer," *Mater. Res. Express*, vol. 4, no. 12, p. 125505, Dec. 2017, doi: 10.1088/2053-1591/aa9dc9.

[10] A. A. Fibriyanti *et al.*, "Improved solar cell and photoresponse performance of $CH_3NH_3PbI_3$ perovskite with ZnO nanorods," *IOP Conf. Ser.: Mater. Sci. Eng.*, vol. 515, p. 012089, Apr. 2019, doi: 10.1088/1757-899X/515/1/012089.

[11] I. B. Elkamel, N. Hamdaoui, A. Mezni, and R. Ajjel, "Photoconduction, dielectric and photoluminescence properties of Cu^{2+}: ZnO nanoparticles elaborated by a polyol method," *Ph. Transit.*, vol. 93, no. 4, pp. 388–406, Mar. 2020, doi: 10.1080/01411594.2020.1734201.

[12] P. Raizada, A. Sudhaik, and P. Singh, "Photocatalytic water decontamination using graphene and ZnO coupled photocatalysts: A review," *Mater. Sci. Energy Technol.*, vol. 2, no. 3, pp. 509–525, Dec. 2019, doi: 10.1016/j.mset.2019.04.007.

[13] H. Pujiarti *et al.*, "Performance of dye sensitized solar cells (DSSCs) with ZnO nanorod electrode in different seed solution," *JPSE (J. Phys. Sci. Eng.)*, vol. 6, no. 2, pp. 77–82, Jul. 2021, doi: 10.17977/um024v6i22021p077.

[14] Y. N. Hendri, Y. Rati, R. Marlina, R. Kurniawan, and Y. Darma, "Polarization behavior of seedless ZnO nanocolumnars grown by DC-unbalanced magnetron sputtering," *Ceram. Int.*, vol. 48, no. 20, pp. 30218–30223, Oct. 2022, doi: 10.1016/j.ceramint.2022.06.294.

[15] B. A. Movchan and A. V. Demchishin, "Structure and properties of thick condensates of nickel, titanium, tungsten, aluminum oxides, and zirconium dioxide in vacuum," *Fiz. Metal. Metalloved.*, vol. 28, pp. 653–660, Oct. 1969. [Online]. Available: https://www.osti.gov/biblio/4181669.

[16] J. A. Thornton, "Structure-zone models of thin films," in *31st Annu. Tech. Symp. Opt. Optoelectron. Appl. Sci. Eng.*, in Modeling of Optical Thin Films, vol. 821, pp. 95–105, Feb. 1988, doi: 10.1117/12.941846.

[17] P. B. Barna and M. Adamik, "Fundamental structure forming phenomena of polycrystalline films and the structure zone models," *Thin Solid Films*, vol. 317, no. 1–2, pp. 27–33, Apr. 1998, doi: 10.1016/S0040-6090(97)00503-8.

[18] R. Kurniawan *et al.*, "Polarization behavior of zinc oxide thin films studied by temperature dependent spectroscopic ellipsometry," *Opt. Mater. Express*, vol. 7, no. 11, pp. 3902–3908, Nov. 2017, doi: 10.1364/OME.7.003902.

[19] P. P. Das *et al.*, "Redistribution of native defects and photoconductivity in ZnO under pressure," *RSC Adv.*, vol. 9, no. 8, pp. 4303–4313, Feb. 2019, doi: 10.1039/C8RA10219H.

[20] M. Zhang *et al.*, "Controlled formation of native defects in ultrapure ZnO for the assignment of green emissions to oxygen vacancies," *J. Phys. Chem. C*, vol. 124, no. 23, pp. 12696–12704, Jun. 2020, doi: 10.1021/acs.jpcc.0c01078.

[21] G. L. Tan, L. K. DeNoyer, R. H. French, M. J. Guittet, and M. Gautier-Soyer, "Kramers–Kronig transform for the surface energy loss function," *J. Electron Spectros. Relat. Phenomena*, vol. 142, no. 2, pp. 97–103, Feb. 2005, doi: 10.1016/j.elspec.2004.09.002.

[22] J. Gong, R. Dai, Z. Wang, and Z. Zhang, "Thickness dispersion of surface plasmon of Ag nano-thin films: Determination by ellipsometry iterated with transmittance method," *Sci. Rep.*, vol. 5, no. 1, p. 9279, Aug. 2015, doi: 10.1038/srep09279.